

Specular Andreev reflection and magnetoresistance in graphene-based ferromagnet–superconductor hybrid systems

This article has been downloaded from IOPscience. Please scroll down to see the full text article.

2008 *J. Phys.: Condens. Matter* 20 335202

(<http://iopscience.iop.org/0953-8984/20/33/335202>)

[View the table of contents for this issue](#), or go to the [journal homepage](#) for more

Download details:

IP Address: 129.252.86.83

The article was downloaded on 29/05/2010 at 13:54

Please note that [terms and conditions apply](#).

Specular Andreev reflection and magnetoresistance in graphene-based ferromagnet–superconductor hybrid systems

Chunxu Bai, Yanling Yang and Xiangdong Zhang

Department of Physics, Beijing Normal University, Beijing 100875,
People's Republic of China

Received 16 January 2008, in final form 16 June 2008

Published 21 July 2008

Online at stacks.iop.org/JPhysCM/20/335202

Abstract

Spin-polarized transport of relativistic electrons through graphene-based ferromagnet/insulator/superconductor single and double junctions has been investigated on the basis of the Dirac–Bogoliubov–de Gennes equation. We have presented a comparative study on two kinds of cases: in the presence and in the absence of specular Andreev reflection. Although both the magnetoresistance (MR) and conductance are oscillating functions of the effective barrier potential and the thickness of the superconductive graphene (SG) layer for the two kinds of cases, some differences in features have also been found. In the presence of specular Andreev reflection, the MR decreases quickly with an increase of the thickness of the SG layer, and negative MR can be observed, which is in contrast to the case for the absence of specular Andreev reflection. It is interesting that the resonance peak of the MR can appear at a certain bias voltage due to the retroreflection crossing over to specular Andreev reflection. This means that the MR can be tuned by an external bias voltage, which benefits spin-polarized electron devices based on graphene materials.

(Some figures in this article are in colour only in the electronic version)

1. Introduction

Recently, there has been a great deal of interest in studying the physical properties of graphene due to the successful fabrication experiment by Novoselov *et al* [1]. Graphene is a monolayer of carbon atoms densely packed in a honeycomb lattice, which can be viewed as either an individual atomic plane pulled out of bulk graphite or unrolled single-wall carbon nanotubes. In graphene, the low energy bands can be described by a two-dimensional Dirac equation centered on the hexagonal corners (Dirac points) of the honeycomb lattice Brillouin zone [2, 3]. The quasiparticle excitations around the Dirac point obey linear Dirac-like energy dispersion. The presence of such Dirac-like quasiparticles is expected to lead to a number of unusual electronic properties in graphene [4–9].

Graphene is not a natural superconductor. However, very recent research has shown that superconductivity can be induced in a graphene layer in the presence of a superconducting

electrode by means of the proximity effect [10–12]. Graphene which possesses superconductivity is called ‘superconductive graphene (SG)’ [10–12]. Consequently, various investigations on transport of electrons through graphene-based superconductor junctions have been undertaken [10–12]. The existence of specular Andreev reflection in these structures has been predicted [10]. Such a specular Andreev reflection process leads to qualitatively different tunneling properties compared with those of the conventional superconductor junctions [11, 12].

In parallel with the above investigations, the ferromagnetism of graphene has also been discussed. The ferromagnetism and spin-polarized states of charge carriers can be induced in the graphene layer by doping and defects [13–16] or adding an external electric field [17] although the graphene is not a natural ferromagnet. In fact, they can also be induced by spin injection in the presence of a ferromagnetic electrode, which is similar to the production of carbon-based magnetism [18, 19]. The previous investigations have shown

that spin injection is an efficient method for obtaining spin-polarized states for some nonmagnetic metals and semiconductors [20]. Similarly, we can put a graphene layer in close proximity to a ferromagnetic insulator such as EuO. Via the magnetic proximity effect, exchange splitting will be induced in the graphene layer [19]. Recent experiments on spin injection in single-layer graphene have extracted a spin relaxation length between 1.5 and 2 μm at room temperature [18]. Graphene which possesses ferromagnetism is called ‘ferromagnetic graphene (FG)’ [21]. Monolayer FG also exhibits some different properties in comparison with the conventional ferromagnets, because they need be described by a Dirac-like equation rather than the usual Schrödinger equation [13–17, 21].

It is natural to ask what kind of phenomenon will occur when we combine FG with SG to construct a graphene-based ferromagnet–superconductor junction. In the past few years, the spin-polarized transport of electrons in conventional ferromagnet–superconductor hybrid systems has been investigated extensively and many interesting results have been obtained [22–29]. Then comes a problem: do the graphene-based ferromagnet–superconductor junctions possess the same properties as the conventional ferromagnet–superconductor junctions?

Considering these problems, in this paper we use the Dirac–Bogoliubov–de Gennes (DBdG) equation to study spin-polarized transport of relativistic electrons through graphene-based ferromagnet/insulator/superconductor (FG/IG/SG) single junctions and ferromagnet/insulator/superconductor/insulator/ferromagnet (FG/IG/SG/IG/FG) double junctions. Here, IG represents the local barrier, which can be implemented by either using the electric field effect or local chemical doping [1, 12]. The conductance and magnetoresistance (MR) in these systems are discussed in detail.

2. A single FG/IG/SG junction

2.1. Theory and model

We first consider a FG/IG/SG junction in a monolayer graphene sheet occupying the xy plane; the schematic potential of the model for the relativistic spin-polarized electrons is shown in figure 1. The growth direction is taken along the x axis. The left FG and right SG are separated by a barrier potential V_0 with width d . Here we assume that the FG electrode has exchange splitting, which is described by $h(x) = h_0\Theta(-x-d)$, where $\Theta(x)$ is the Heaviside step function. The potential profile of the system is given by $V(x) = V_0\Theta(-x)\Theta(x+d) - U_0\Theta(x)$. For the SG electrode, neglecting the self-consistency of the superconducting pair potential, $\Delta(x)$ is taken in the form $\Delta(x) = \Delta_0 e^{i\phi}\theta(x)$, where Δ_0 and ϕ are the amplitude and phase of the induced superconducting order parameter, respectively. We focus here on the case where the width (along the y direction) of the graphene strip, W , is much larger than d , that is to say $d \ll W$. In this case the details of the microscopic description of the strip edges becomes irrelevant. The charge carriers in the

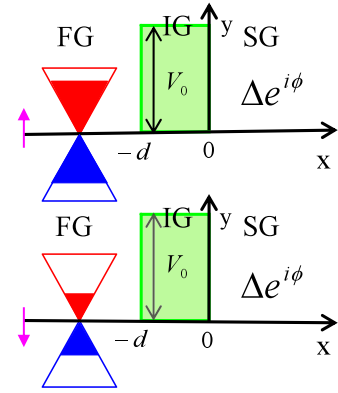


Figure 1. A schematic representation of the energy bands and potential profile in a FG/IG/SG junction. Top for spin up electrons; bottom for spin down electrons. Note that we take the limit of the thin barrier, namely, $V_0 \rightarrow \infty$ and $d \rightarrow 0$, such that $\chi = V_0 d / v_F \hbar$ remains finite.

present system can then be described by the following DBdG equation [10]:

$$\begin{pmatrix} H_0 - h(x)\rho_\sigma & \Delta(x) \\ \Delta^*(x) & -H_0 + h(x)\rho_{\bar{\sigma}} \end{pmatrix} \begin{pmatrix} u_{a\sigma} \\ v_{\bar{a}\bar{\sigma}} \end{pmatrix} = E \begin{pmatrix} u_{a\sigma} \\ v_{\bar{a}\bar{\sigma}} \end{pmatrix}, \quad (1)$$

where $u_{a\sigma} = (\psi_{Aa\sigma}, \psi_{Ba\sigma})$ represents the two-dimensional spinor of the electron in one valley a with spin σ and $v_{\bar{a}\bar{\sigma}} = (\psi_{A\bar{a}\bar{\sigma}}^*, -\psi_{B\bar{a}\bar{\sigma}}^*)$ is the two-dimensional spinor of the hole in one valley \bar{a} with spin $\bar{\sigma}$, the index a denotes K or K' for electrons or holes near K and K' points, \bar{a} takes values $K'(K)$ for $a = K(K')$, ρ_σ is 1 (-1) for up (down) spins, and the Hamiltonian H_0 is given by

$$H_0 = -i\hbar v_F [\sigma_x \partial_x + \text{sgn}(a)\sigma_y \partial_y] + V(x) - E_F, \quad (2)$$

where v_F denotes the Fermi velocity of the quasiparticles in the graphene, E_F represents the Fermi energy, and $\text{sgn}(a)$ takes values $+$ ($-$) for $a = K$ (K'). In order to solve the transport problem in the FG/IG/SG junction (sketched in figure 1), we assume that the incident electron with spin σ and the reflected hole with spin $\bar{\sigma}$ propagate at angles of α_σ and $\alpha'_{\bar{\sigma}}$ along x axis. For a spin up electron incident on the junction from the left FG electrode with an energy ε and transverse momentum q , the wavefunctions in the three regions, taking into account both Andreev and normal reflection processes, can be written as [10–12]

$$\begin{aligned} \Psi_1 &= \Psi_{F\sigma}^{e+} + r \Psi_{F\sigma}^{e-} + r_A \Psi_{F\bar{\sigma}}^{h-}, & \text{in the FG region} \\ \Psi_2 &= p \Psi_{I\sigma}^{e+} + q \Psi_{I\sigma}^{e-} + m \Psi_{I\bar{\sigma}}^{h+} + n \Psi_{I\bar{\sigma}}^{h-}, & \text{in the IG region} \\ \Psi_3 &= t \Psi_S^{e+} + t' \Psi_S^{h+} & \text{in the SG region,} \end{aligned} \quad (3)$$

where r and r_A are the amplitudes of normal and Andreev reflections in the FG region, t and t' are the amplitudes of electron-like quasiparticle and hole-like quasiparticle in the SG region, respectively. p , q , m , and n are the amplitudes of spin σ electrons and spin $\bar{\sigma}$ holes in the IG region. $\Psi_{F\sigma}^{e\pm}$ and $\Psi_{F\bar{\sigma}}^{h\pm}$ represent the wavefunctions in the FG region traveling along the $\pm x$ direction with a transverse momentum $k_{y\sigma} = q$ and

energy ε for electrons and holes, respectively. They can be expressed in the following form:

$$\begin{aligned}\Psi_{F\sigma}^{e\pm} &= (1, \pm e^{\pm i\alpha_\sigma}, 0, 0) e^{i(\pm k_\sigma x + qy)} / \sqrt{\cos(\alpha_\sigma)} \\ \Psi_{F\bar{\sigma}}^{h\pm} &= (0, 0, 1, \mp e^{\pm i\alpha'_{\bar{\sigma}}}) e^{i(\pm k'_{\bar{\sigma}} x + qy)} / \sqrt{\cos(\alpha'_{\bar{\sigma}})} \\ \alpha_\sigma &= \arcsin[\hbar v_F q / (\varepsilon + E_F + \rho_\sigma h_0)], \\ \alpha'_{\bar{\sigma}} &= \arcsin[\hbar v_F q / (\varepsilon - E_F - \rho_{\bar{\sigma}} h_0)].\end{aligned}\quad (4)$$

Here $k_\sigma = (\varepsilon + E_F + \rho_\sigma h_0) \times \cos(\alpha_\sigma) / \hbar v_F$ and $k'_{\bar{\sigma}} = (\varepsilon - E_F - \rho_{\bar{\sigma}} h_0) \times \cos(\alpha'_{\bar{\sigma}}) / \hbar v_F$ are the momenta along the x axis. Note that a critical incident angle should be considered in the scattering process; it is given by $\alpha_{C\sigma} = \arcsin[(\varepsilon - E_F - \rho_{\bar{\sigma}} h_0) / (\varepsilon + E_F + \rho_\sigma h_0)]$. When the incident angle of the electron is larger than the critical incident angle ($|\alpha_\sigma| > \alpha_{C\sigma}$), there are no propagating AR solutions and one should take $\alpha'_{\bar{\sigma}} = \text{sgn}(\alpha_\sigma) (\frac{\pi}{2} \text{sgn}(\varepsilon - E_F - \rho_{\bar{\sigma}} h_0) - \text{i} \text{arccosh} |\frac{\sin \alpha_\sigma}{\sin \alpha_{C\sigma}}|)$. However, the evanescent AR solutions in the calculations for such a case have to be included to ensure the appropriate current conservation. $\Psi_{I\sigma}^{e\pm}$ and $\Psi_{I\bar{\sigma}}^{h\pm}$ represent the wavefunctions in the IG region, which are given by

$$\begin{aligned}\Psi_{I\sigma}^{e\pm} &= (1, \pm e^{\pm i\theta_\sigma}, 0, 0) e^{i(\pm k_\sigma x + qy)} / \sqrt{\cos(\alpha_\sigma)}, \\ \Psi_{I\bar{\sigma}}^{h\pm} &= (0, 0, 1, \mp e^{\pm i\theta'_{\bar{\sigma}}}) e^{i(\pm k'_{\bar{\sigma}} x + qy)} / \sqrt{\cos(\alpha'_{\bar{\sigma}})},\end{aligned}\quad (5)$$

where θ_σ ($\theta'_{\bar{\sigma}}$) is defined as $\theta_\sigma(\theta'_{\bar{\sigma}}) = \arcsin[\hbar v_F q / (\varepsilon + (-)(E_F + \rho_\sigma(\rho_{\bar{\sigma}}) - V_0))]$ and $k_{I\sigma}$ ($k'_{I\bar{\sigma}}$) = $[\varepsilon - (+)(E_F + \rho_\sigma(\rho_{\bar{\sigma}}) - V_0)] \times \cos[\theta_\sigma(\theta'_{\bar{\sigma}})] / \hbar v_F$. In particular, we define a thin barrier as one with $V_0 \rightarrow \infty$ and $d \rightarrow 0$ such that $\chi = V_0 d / v_F \hbar$ remains finite. Note that in the limit of the thin barrier, $\theta_\sigma, \theta'_{\bar{\sigma}} \rightarrow 0$ and $k_{I\sigma} d, k'_{I\bar{\sigma}} d \rightarrow \chi$ [11].

In equation (3) $\Psi_S^{e\pm}$ and $\Psi_S^{h\pm}$ represent the wavefunctions of mixture DBdG quasiparticles in the SG region, which can be expressed as

$$\begin{aligned}\Psi_S^{e\pm} &= (e^{-i\beta}, \mp e^{-i(\beta \mp \gamma)}, e^{-i\phi}, \mp e^{-i(\phi \mp \gamma)}) e^{i(\pm k_S x + qy) \mp \kappa x}, \\ \Psi_S^{h\pm} &= (e^{i\beta}, \pm e^{i(\beta \mp \gamma)}, e^{-i\phi}, \pm e^{-i(\phi \pm \gamma)}) e^{i(\mp k_S x + qy) \mp \kappa x},\end{aligned}\quad (6)$$

where the momentum k_S along the x axis, the incidence angle γ for the quasiparticles, the localization length κ , and parameter β are defined by

$$\begin{aligned}k_S &= \sqrt{(U_0 + E_F)^2 / (\hbar v_F)^2 - q^2}, \\ \gamma &= \arcsin[\hbar v_F q / (E_F + U_0)], \\ \kappa &= (U_0 + E_F) \Delta_0 \sin \beta / (\hbar v_F)^2 k_S, \\ \beta &= \begin{cases} \arccos(\varepsilon / \Delta_0) & \varepsilon < \Delta_0, \\ -i \text{arccosh}(\varepsilon / \Delta_0) & \varepsilon > \Delta_0. \end{cases}\end{aligned}\quad (7)$$

Here U_0 represents the electrostatic potential which may be adjusted independently via a gate voltage or doping. Applying the continuity of the wavefunctions at the boundaries, $\psi_1(-d)|_{d \rightarrow 0} = \psi_2(-d)|_{d \rightarrow 0}$ and $\Psi_2(0) = \Psi_3(0)$, the following transfer matrix is obtained:

$$\begin{pmatrix} 1 + r \\ e^{i\alpha_\sigma} - r e^{-i\alpha_\sigma} \\ r_A \\ r_A e^{-i\alpha'_{\bar{\sigma}}} \end{pmatrix} = \begin{pmatrix} e^{-i\chi} & e^{i\chi} & 0 & 0 \\ e^{-i\chi} & -e^{i\chi} & 0 & 0 \\ 0 & 0 & e^{-i\chi} & e^{i\chi} \\ 0 & 0 & -e^{-i\chi} & e^{i\chi} \end{pmatrix}^{-1} \begin{pmatrix} 1 & 1 & 0 & 0 \\ 1 & -1 & 0 & 0 \\ 0 & 0 & 1 & 1 \\ 0 & 0 & -1 & 1 \end{pmatrix} \begin{pmatrix} e^{-i\beta} & e^{i\beta} \\ -e^{i(\gamma - \beta)} & e^{-i(\gamma - \beta)} \\ e^{-i\phi} & e^{-i\phi} \\ -e^{i(\gamma - \phi)} & e^{-i(\gamma + \phi)} \end{pmatrix} \begin{pmatrix} t \\ t' \end{pmatrix}.\quad (8)$$

Then the coefficients in equation (3) can be calculated. If we take $h_0 = 0$, that is to say, there is no ferromagnetism, equation (8) gives the same results as [11].

After the transmission coefficients are obtained, the tunneling conductance at zero temperature can be calculated by means of the Blonder–Tinkham–Klapwijk formula [10, 11, 30],

$$G(ev) = G_0 \int_0^{\pi/2} (1 - |r|^2 + |r_A|^2) \cos[\alpha_\sigma] d\alpha_\sigma, \quad (9)$$

where $G_0 = 2e^2 N(ev) / h$ is the ballistic conductance of metallic graphene, ev is the bias voltage, and $N(ev) = (E_F + \varepsilon)w / (\pi \hbar v_F)$ denotes the number of available channels for the graphene sample with width w . Using equation (8) and (9) the conductance for the single junction can be obtained easily by numerical calculation.

2.2. Numerical results and discussion

Here we present the calculated results for Andreev reflection coefficients and the tunneling conductance for the FG/IG/SG junction. In general, it is very difficult to reach the regime $E_F \ll \Delta_0$ in experiments [10]. So, we only consider the case of $E_F \gg \Delta_0$ (case I) and the regime of comparable E_F and Δ_0 (case II) in the following. For case I, only normal Andreev reflection (retroreflection) plays a role in the process. For case II, both normal Andreev reflection and specular Andreev reflection play roles, that is to say, the retroreflection crosses over to specular Andreev reflection [10]. The tunneling coefficients through the FG/IG/SG junction as a function of incident angle α_σ for two kinds of cases are plotted in figure 2.

Figures 2(a) and (b) correspond to the cases of the normal reflection and Andreev reflection for case I, respectively, while figures 2(c) and (d) represent the corresponding cases for case II. The solid line, dashed line and dash-dotted line describe the results for unpolarized, spin up, and spin down electrons, respectively. Here $E_F = 10^3 \Delta_0$ for case I and $E_F = \Delta_0$ for case II are taken. The other parameters used in the calculations are $eV/\Delta = 0.5$, $U_0/E_F = 10$, and $\chi = \pi/8$. It is seen from the figures that the different features appear for the two kinds of cases. For case I with the limit of thin barriers, there is not much difference between the three kinds of curves, for unpolarized, spin up, and spin down electrons. In contrast, separations for the three kinds of curves can be clearly observed for case II even for small h_0 ($h_0 = 0.2$ in figures 2(c) and (d)). This is because specular Andreev reflection (the interband electron–hole conversion) [10] appears for case II, which leads to the critical Andreev reflection angle

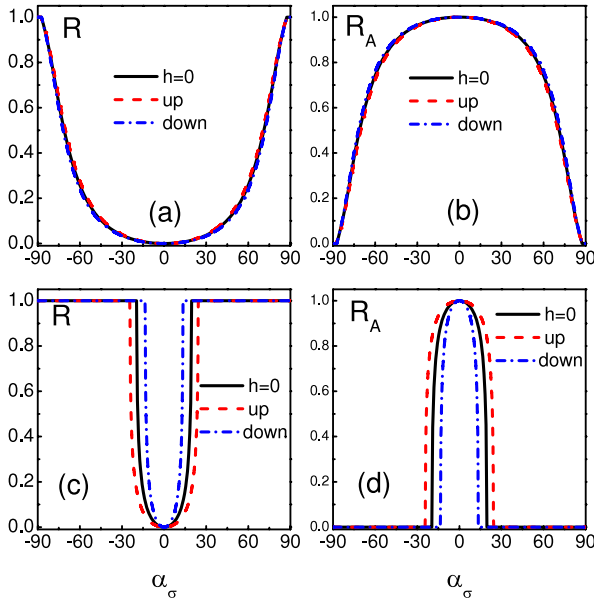


Figure 2. Normal reflection R and Andreev reflection R_A through a single FG/IG/SG junction as a function of the incident angle for unpolarized electrons (solid line), spin up electrons (dashed line) and spin down electrons (dash-dotted line). $E_F = 10^3 \Delta$ for (a) and (b); $E_F = \Delta$ for (c) and (d). The other parameters are taken as $eV/\Delta = 0.5$, $U_0/E_F = 10$, $\chi = \pi/8$ and $h_0/E_F = 0.2$.

$\alpha_{C\sigma}$ ($\alpha_{C\sigma} = \arcsin[|\varepsilon - E_F - \rho_{\bar{\sigma}} h_0|/(\varepsilon + E_F + \rho_{\sigma} h_0)]$) being very sensitive to the value of h_0 . In such a process, the retroreflection crosses over to specular Andreev reflection. However, for case I, specular Andreev reflection is absent and the angle $\alpha_{C\sigma}$ can be simplified to $\alpha_{C\sigma} = \arcsin[[-E_F - \rho_{\bar{\sigma}} h_0]/(E_F + \rho_{\sigma} h_0)]$. It is nearly independent on h_0 and almost reaches $\pi/2$ at $eV/\Delta = 0.5$ due to the large value of E_F . This is why we cannot find the separations for the three kinds of curves in figures 2(a) and (b).

These differences in the transmission coefficients lead directly to differences in conductance. Figures 3(a) and (b) show the differential conductance as a function of bias voltage for two kinds of cases, respectively. For the case with $h_0 = 0$, our results are identical with those in [11]. When the spin-polarized state is considered, separable conductances for spin up and spin down electrons appear for case II, while there is no difference between the conductance of spin up and spin down electrons for case I. This can be seen more clearly from figure 4.

Figures 4(a) and (b) display the tunneling conductance as a function of the effective barrier potential χ at $eV/\Delta = 0.5$ for cases I and II, respectively. The solid line corresponds to the case of spin up electrons and open circles to that of spin down electrons. A large separation between the solid line and the open circles is found in figure 4(b), while their superposition is observed in figure 4(a) again. It is also clearly seen that all cases exhibit oscillation behaviors, which are similar to those of graphene-based metal-insulator-superconductor junctions in the limit of a thin barrier. They arise from transmission resonance ($r = 0$, $|r_A| = 1$) for the condition $\beta - 2\chi = n\pi$ and $n = 0, \pm 1, \pm 2, \dots$. This is directly related to the Klein

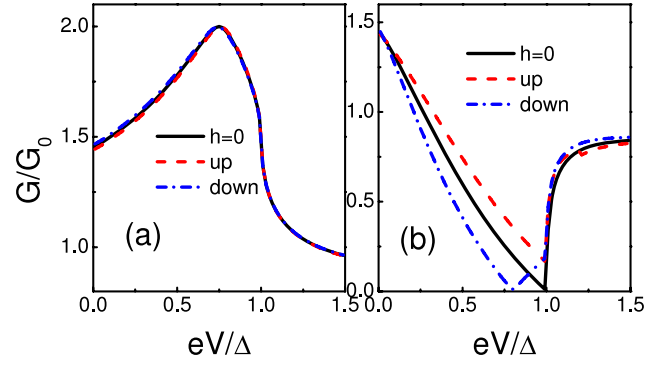


Figure 3. Tunneling conductance of a FG/IG/SG junction as a function of bias voltage for unpolarized electrons (solid line), spin up electrons (dashed line) and spin down electrons (dash-dotted line). (a) Corresponds to $E_F = 10^3 \Delta$ and (b) to $E_F = \Delta$. The other parameters are identical to those of figure 2.

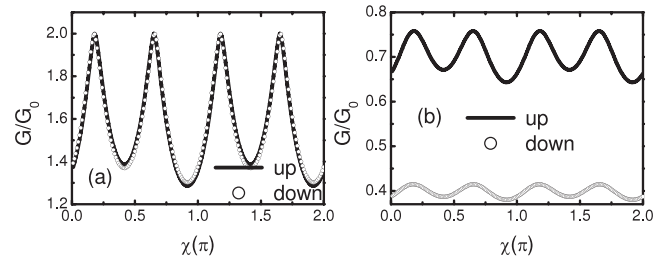


Figure 4. Tunneling conductance of a FG/IG/SG junction as a function of the effective barrier potential χ for spin up electrons (solid line) and spin down electrons (open circle). (a) Corresponds to $E_F = \Delta$ and (b) to $E_F = 10^3 \Delta$. The other parameters are identical to those in figure 2.

tunneling [9]. The conductance exhibits a $\pi/2$ or π oscillation period at a fixed energy as a function of χ for $U_0 \gg E_F$ and $U_0 = 0$, respectively. Here $U_0 = 10E_F$ is taken. Thus, the oscillation features in figure 4 lie between the case with $U_0 \gg E_F$ and that with $U_0 = 0$.

The above results are only for the case of the FG/IG/SG single junction. Some differences between case I and case II have been found. In fact, such differences can be found more remarkably in the FG/IG/SG/IG/FG double junctions.

3. A FG/IG/SG/IG/FG double junction

3.1. Theory and model

Now let us consider a FG/IG/SG/IG/FG double junction in the graphene sheet occupying the xy plane, in which the left and right electrodes are made of the same FG, and they are separated from the central SG by two identical thin barriers as shown in figure 5. The growth direction is also taken along the x axis. The region IG, modeled by a barrier potential V_0 , extends from $x = -d$ to 0 and $x = l$ to $l + d$, the FG region occupies $x < -d$ and $x > l + d$, while the superconducting region occupies $0 < x < l$. Here we assume that the two FG electrodes have the same exchange splitting, which is described by $h(x) = h_0[\Theta(-x) \pm \Theta(x - l)]$ where the plus (minus) sign corresponds to the parallel (P) (antiparallel (AP))

configuration of magnetizations. The potential profile $V(x)$ in the FG, IG and SG regions may be adjusted independently via a gate voltage or doping; it is taken as

$$V(x) = \begin{cases} -U_0 & 0 < x < l \\ V_0 & -d < x < 0, \quad l < x < l+d \\ 0 & x < -d, \quad x > l+d. \end{cases} \quad (10)$$

The other parameters are taken the same to those in the FG/IG/SG single junction and the charge carriers are also described by equations (1) and (2). For a spin σ electron incident on the junction from the left FG electrode with an energy ε and transverse momentum q , the wavefunctions in the five regions can then be written as

$$\begin{aligned} \Psi_1 &= \Psi_{F\sigma}^{e+} + r\Psi_{F\sigma}^{e-} + r_A\Psi_{F\sigma}^{h-}, \\ \Psi_2 &= \Psi_4 = p\Psi_{l\sigma}^{e+} + q\Psi_{l\sigma}^{e-} + m\Psi_{l\sigma}^{h+} + n\Psi_{l\sigma}^{h-}, \\ \Psi_3 &= e\Psi_S^{e+} + f\Psi_S^{e-} + g\Psi_S^{h+} + h\Psi_S^{h-}, \\ \Psi_5 &= t\Psi_{F\sigma(\bar{\sigma})}^{e+} + t'\Psi_{F\sigma(\bar{\sigma})}^{h+}, \end{aligned} \quad (11)$$

where r and r_A are the amplitudes of normal and Andreev reflections, respectively; t and t' are the amplitudes of spin σ ($\bar{\sigma}$) electrons and spin $\bar{\sigma}$ (σ) holes for the P (AP) configuration of magnetizations in the FG region; e, f, g and h are the amplitudes of electron-like and hole-like quasiparticles in the SG region; p, q, m , and n are the amplitudes of spin σ electrons and spin $\bar{\sigma}$ holes in the IG regions. All the amplitudes in equation (11) can be determined through the following boundary conditions:

$$\begin{aligned} \psi_1(-d)|_{d \rightarrow 0} &= \psi_2(-d)|_{d \rightarrow 0}, \quad \Psi_2(0) = \Psi_3(0), \\ \Psi_3(l) &= \Psi_4(l), \quad \psi_4(l+d)|_{d \rightarrow 0} = \Psi_5(l+d)|_{d \rightarrow 0}. \end{aligned} \quad (12)$$

Then the transfer matrix for the present double junctions can be obtained as

$$\begin{aligned} &\begin{pmatrix} e^{ik_{F\sigma}L(1)} + re^{-ik_{F\sigma}L(1)} \\ e^{ik_{F\sigma}L(1)+i\alpha_\sigma} - re^{-ik_{F\sigma}L(1)-i\alpha_\sigma} \\ r_A e^{-ik'_{F\sigma}L(1)} \\ r_A e^{-ik'_{F\sigma}L(1)-i\alpha'_{\bar{\sigma}}} \end{pmatrix} \\ &= \begin{pmatrix} e^{-i\chi} & e^{i\chi} & 0 & 0 \\ e^{-i\chi} & -e^{i\chi_\sigma} & 0 & 0 \\ 0 & 0 & e^{-i\chi} & e^{i\chi} \\ 0 & 0 & -e^{-i\chi} & e^{i\chi} \end{pmatrix} S'_{(x)} \\ &\times \begin{pmatrix} e^{ik_{F\sigma(\bar{\sigma})}L(4)} & 0 \\ e^{ik_{F\sigma(\bar{\sigma})}L(4)+i\alpha_{\sigma(\bar{\sigma})}} & 0 \\ 0 & e^{ik'_{F\sigma(\bar{\sigma})}L(4)} \\ 0 & -e^{ik'_{F\sigma(\bar{\sigma})}L(4)+i\alpha'_{\sigma(\bar{\sigma})}} \end{pmatrix} \begin{pmatrix} t \\ t' \end{pmatrix}, \end{aligned} \quad (13)$$

where

$$S'_{(x)} = S_{(x=L(2))}^{-1} S_{(x=L(2))} S_{(x=L(3))}^{-1} S_{(x=L(3))}^*, \quad (14)$$

$$S_{(x=L(2))} = \begin{pmatrix} e^{ik_{l\sigma}L(2)} & e^{-ik_{l\sigma}L(2)} & 0 & 0 \\ e^{ik_{l\sigma}L(2)+i\theta_\sigma} & -e^{-ik_{l\sigma}L(2)-i\theta_\sigma} & 0 & 0 \\ 0 & 0 & e^{ik'_{l\sigma}L(2)} & e^{-ik'_{l\sigma}L(2)} \\ 0 & 0 & -e^{ik'_{l\sigma}L(2)+i\theta'_{\bar{\sigma}}} & e^{-ik'_{l\sigma}L(2)-i\theta'_{\bar{\sigma}}} \end{pmatrix}, \quad (15)$$

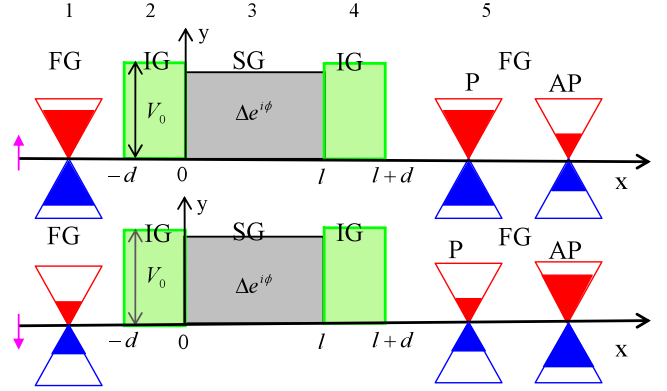


Figure 5. The schematic representation of energy bands and the potential profile in the P and AP alignments for a FG/IG/SG/IG/FG double junction. Top for spin up electrons; bottom for spin down electrons.

$$S_{(x=L(2))}^* = \begin{pmatrix} Ae^{-i\beta} & Be^{-i\beta} & Ce^{i\beta} & De^{i\beta} \\ -Ae^{-i(\beta-\gamma)} & Be^{-i(\beta+\gamma)} & -Ce^{i(\beta+\gamma)} & De^{i(\beta-\gamma)} \\ Ae^{-i\phi} & Be^{-i\phi} & Ce^{-i\phi} & De^{-i\phi} \\ -Ae^{i(\gamma-\phi)} & Be^{-i(\gamma+\phi)} & -Ce^{i(\gamma-\phi)} & De^{-i(\gamma+\phi)} \end{pmatrix}. \quad (16)$$

Here $A = e^{(ik_S - \kappa)L(2)}$, $B = e^{-(ik_S - \kappa)L(2)}$, $C = e^{(ik_S + \kappa)L(2)}$ and $D = e^{-(ik_S + \kappa)L(2)}$. $L(1), L(2), L(3)$ and $L(4)$ are taken as 0, l and l , respectively. Adopting a the method similar to that used to obtain $S_{(x=L(2))}$ and $S_{(x=L(2))}^*$, we can get the expressions for $S_{(x=L(3))}$ and $S_{(x=L(3))}^*$. After transmission coefficients are obtained by solving equation (16), the tunneling conductance for the double junctions can be calculated using equation (9), like in the case of the single junction. The tunneling conductance is the sum of those of the two spin channels and depends on the magnetization configuration of the two FG electrodes. For the P configuration, $G_P = G_{\uparrow\uparrow} + G_{\downarrow\downarrow}$; while for the AP configuration, $G_{AP} = G_{\uparrow\downarrow} + G_{\downarrow\uparrow}$. Then the MR, $MR = (G_P - G_{AP})/G_P$, can be calculated easily.

3.2. Numerical results and discussion

An important difference for the FG/IG/SG/IG/FG double junctions in comparison with the FG/IG/SG single junction is that large oscillation MR can be found in the former. We mainly focus on the discussion of such properties of double junctions in the following. Like in the discussion of the single junction, we consider two kinds of cases: case I for $E_F \gg \Delta_0$ and case II for $E_F = \Delta_0$. The MRs of tunneling of spin-polarized electrons through the FG/IG/SG/IG/FG double junctions as a function of the thickness of SG for case I and case II are plotted in figures 6(a) and (c), respectively. Both of them exhibit oscillation features. In order to explain such features, we also plot the corresponding tunneling conductances (G_P and G_{AP}) for the two kinds of cases in figures 6(b) and (d), respectively. Solid lines correspond to G_P and dashed lines to G_{AP} . All of them oscillate with the change of the SC layer due to the effects of interference between electron-like and hole-like quasiparticles in the SC.

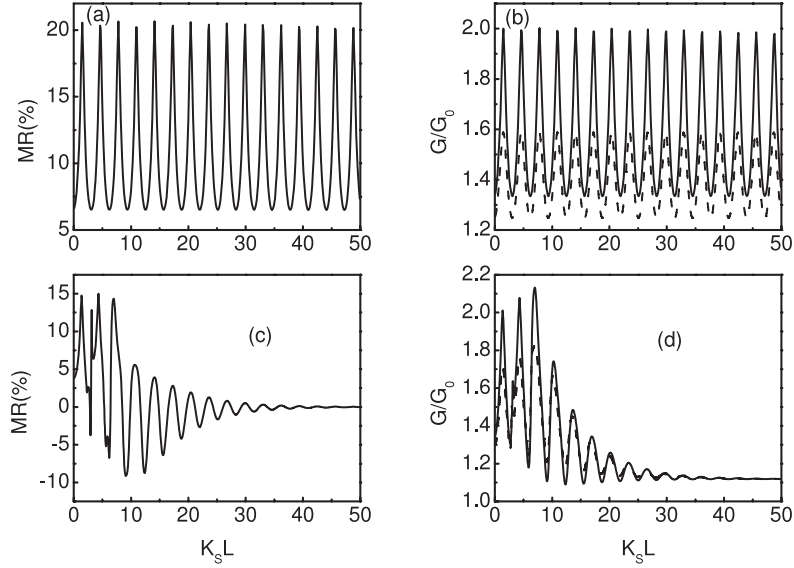


Figure 6. Tunneling magnetoresistance (MR) ((a) and (c)) and conductance ((b) and (d)) as a function of the SG thickness ($k_s L$). (a) and (b) correspond to the case with $E_F = 10^3 \Delta$, and (c) and (d) to that with $E_F = \Delta$. Solid lines in (b) and (d) represent the conductance of the P configuration (G_P) and dashed lines are for the AP configuration (G_{AP}). The other parameters are identical to those of figure 2.

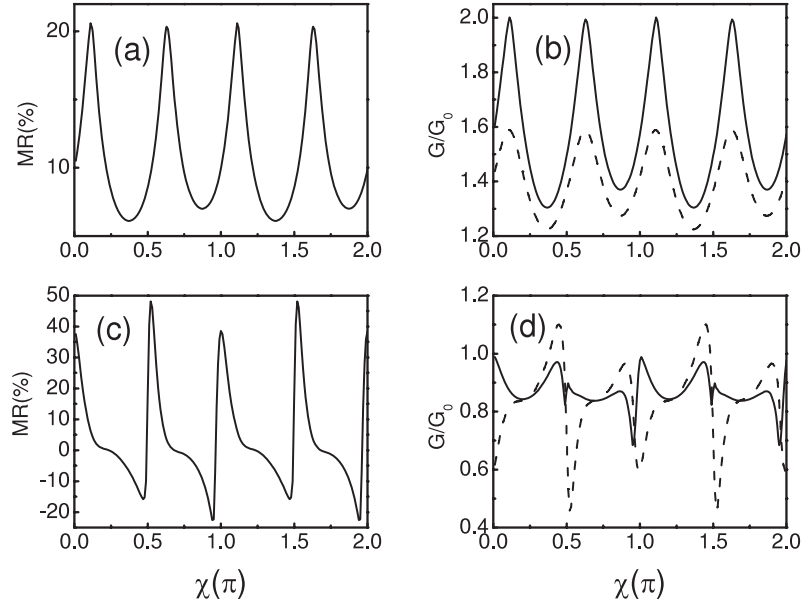


Figure 7. Tunneling magnetoresistance (MR) ((a) and (c)) and conductance ((b) and (d)) as a function of the effective barrier potential χ . (a) and (b) correspond to the case with $E_F = 10^3 \Delta$, and (c) and (d) to that with $E_F = \Delta$. Solid lines in (b) and (d) represent the conductance of the P configuration (G_P) and dashed lines are for the AP configuration (G_{AP}). Here $eV/\Delta = 0.9$ and $k_s l = 15$. The other parameters are identical to those in figure 2.

The oscillation periods for G_P and G_{AP} are nearly the same. This leads to the oscillation of the MR with the same periods.

At the same time, we also find that their oscillation amplitudes decay with increase of the thickness of the SG layer due to the existence of the exponential decay term $e^{\pm \kappa l}$ in equation (13). However, the decay features for case I and case II are different. The oscillation amplitudes of the MR and conductance decrease quickly with increase of the thickness of the SG layer for case II, while they decay slowly for case I. This is because the parameter κ in the exponential term $e^{\pm \kappa l}$ is equal to $(\Delta/\hbar v) \sin \beta$ in the $U_0 \gg E_F$ limit. It is bigger for

$E_F = \Delta$ (case II) than for $E_F = 10^3 \Delta$ (case I), which results in quick decreases of the MR and conductance in case II.

The other difference between case I and case II is that negative MR can appear in the latter, while MR always exhibits positive values in the former. This can be understood from the difference of conductances G_P and G_{AP} in figure 6(d). For case II, the value of G_{AP} can become larger than that of G_P for some cases with a certain $k_s L$ due to the retroreflection crossing over to specular Andreev reflection, which makes the MR become negative.

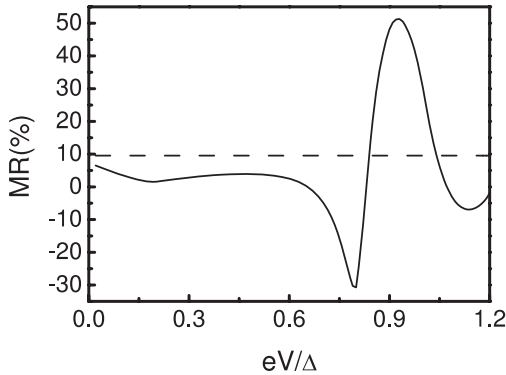


Figure 8. Tunneling magnetoresistance (MR) as a function of bias voltage for the case with $E_F = 10^3 \Delta$ (dashed line) and that with $E_F = \Delta$ (solid line). Here $\chi = 0.52\pi$. The other parameters are identical to those of figure 7.

The MR can be tuned not only via the middle SG layer, but also by changing the effective barrier potential χ . Figures 7(a) and (c) show the MR as a function of the effective barrier potential χ for case I and case II, respectively, and the corresponding conductances are given in figures 7(b) and (d). All of them are oscillating functions of χ , and negative MR is observed in case II again. The physical origin for such a phenomenon can be understood as similar to that of the above analysis as regards the single FG/IG/SG junction. The oscillation periods are also determined by similar methods.

The MR not only oscillates with the change of the effective barrier potential and the SG layer, but also can be changed using external voltage for case II. The solid line in figure 8 represents such a case. Figure 8 displays the MR as a function of bias voltage for case I (dashed line) and case II (solid line). It is clearly seen that the large resonant peak appears at a certain bias voltage for case II. Such a resonance is the result of competition between the external voltage and the retroreflection crossing over to specular Andreev reflection. This means that the MR in case II can be tuned using the bias voltage. This is in sharp contrast to the phenomenon in case I where the MR stays nearly constant with change of the bias voltage.

4. Summary

On the basis of the Dirac–Bogoliubov–de Gennes equation and transfer matrix method, we have investigated the spin-polarized transport of relativistic electrons through FG/IG/SG single and double junctions. The conductance and MR in these systems have been calculated. The comparative results for two kinds of cases—in the presence or the absence of specular Andreev reflection—have been presented. We have found that separate conductance of spin-polarized electrons and large MR can be obtained even at very small exchange splitting. Although the MR and conductance are both oscillating functions of the effective barrier potential and the thickness of the SG layer for the two kinds of cases, some different features have also been observed. In the presence of specular Andreev reflection, the MR decreases quickly

with increase of the thickness of the SG layer and negative MR can be obtained. This is in contrast to the case in the absence of specular Andreev reflection, where the MR is always positive and decreases slowly with change of the SG layer. We have also found that the resonance peak of the MR can appear at a certain bias voltage in the presence of specular Andreev reflection; this is caused by the competition between the external voltage and the retroreflection crossing over to specular Andreev reflection. This means that the MR can be tuned using the external bias voltage, which benefits spin-polarized electron devices based on graphene materials.

All these predictions should be experimentally observable, because the FG electrode, SG layer and local barrier can be realized by using the methods proposed in [10–19]. However, we have to point out that some effects, such as the spatial variation of the pair potential in the SG due to proximity effects and the spin flip of the charge carriers, have been neglected in our theory. In addition, we limited our calculations by applying the condition of zero temperature. Inclusion of the other effects would be necessary for a complete theory, which merits further study.

Acknowledgments

This work was supported by the National Natural Science Foundation of China (Grant No. 10674017) and the National Key Basic Research Special Foundation of China under Grant 2007CB613205. The project was also sponsored by NCET and RFDP.

References

- [1] Novoselov K S, Geim A K, Morozov S V, Jiang D, Zhang Y, Dubonos S V, Grigorieva I V and Firsov A A 2004 *Science* **306** 666
- [2] Wallace P R 1947 *Phys. Rev.* **71** 622
- [3] For a review, see Ando T 2005 *J. Phys. Soc. Japan* **74** 777
- [4] Novoselov K S, Geim A K, Morozov S V, Jiang D, Katsnelson M L, Grigorieva I V, Dubonos S V and Firsov A A 2005 *Nature* **438** 197
- [5] Novoselov K S, Geim A K, Morozov S V, Jiang D, Katsnelson M L, Grigorieva I V, Dubonos S V and Firsov A A 2006 *Nat. Phys.* **2** 177
- [6] Zhang Y, Tan Y W, Stormer H L and Kim P 2005 *Nature* **438** 201
- [7] Gusynin V P and Sharapov S G 2005 *Phys. Rev. Lett.* **95** 146801
- [8] McCann E and Falko V 2006 *Phys. Rev. Lett.* **96** 086805
- [9] Tworzydlo J, Trauzettel B, Titov M, Rycerz A and Beenakker C W J 2006 *Phys. Rev. Lett.* **96** 246802
- [10] Katsnelson M I, Novoselov K S and Geim A K 2006 *Nat. Phys.* **2** 620
- [11] Pereira J M, Vasilopoulos P Jr and Peeters F M 2007 *Appl. Phys. Lett.* **90** 132122
- [12] Bai C and Zhang X 2007 *Phys. Rev. B* **76** 075430
- [13] Beenakker C W J 2006 *Phys. Rev. Lett.* **97** 067007
- [14] Bhattacharjee S and Sengupta K 2006 *Phys. Rev. Lett.* **97** 217001
- [15] Linder J and Sudbø A 2007 *Phys. Rev. Lett.* **99** 147001
- [16] Titov M and Beenakker C W J 2006 *Phys. Rev. B* **74** R041401
- [17] Peres N M R, Guinea F and Castro Neto A H 2005 *Phys. Rev. B* **72** 174406

[14] Vozmediano M A H, López-Sancho M P, Stauber T and Guinea F 2005 *Phys. Rev. B* **72** 155121

[15] Dugaev V K, Litvinov V I and Barnas J 2006 *Phys. Rev. B* **74** 224438

[16] Oleg Yazyev V and Lothar H 2007 *Phys. Rev. B* **75** 125408

[17] Son Y-W, Cohen M L and Louie S G 2006 *Nature* **444** 347

[18] Tombros N, Jozsa C, Popinciuc M, Jonkman H T and van Wees B J 2007 *Nature* **448** 571

Makarova T and Palacio F (ed) 2005 *Carbon-Based Magnetism: An Overview of Metal Free Carbon-Based Compounds and Materials* (Amsterdam: Elsevier)

[19] Haugen H, Huertas-Hernando D and Brataas A 2007 *Preprint cond-mat* **07073976**

[20] Zutic I, Fabian J and Sarma S D 2004 *Rev. Mod. Phys.* **76** 323

[21] Bai C and Zhang X 2008 *Phys. Lett. A* **372** 725

[22] de Jong M J M and Beenakker C W J 1995 *Phys. Rev. Lett.* **74** 1657

[23] Upadhyay S K, Palanisami A, Louie R N and Buhrman R A 1998 *Phys. Rev. Lett.* **81** 3247

[24] Zhu J X, Friedman B and Ting C S 1999 *Phys. Rev. B* **59** 9558

[25] Bozovic M and Radovic Z 2002 *Phys. Rev. B* **66** 134524

[26] Yamashita T, Imamura H, Takahashi S and Maekawa S 2003 *Phys. Rev. B* **67** 094515

[27] Dong Z C, Shen R, Zheng Z M, Xing D Y and Wang Z D 2003 *Phys. Rev. B* **67** 134515

[28] Soulé R J *et al* 1998 *Science* **282** 85

[29] Zutic I and Valls O T 1999 *Phys. Rev. B* **60** 6320

Zutic I and Valls O T 2000 *Phys. Rev. B* **61** 1555

[30] Blonder G E, Tinkham M and Klapwijk T M 1982 *Phys. Rev. B* **25** 4515